Insertion of Poly(acrylamide) Disc-Columnar Liquid Crystals as a Functional Template in Organic Photovoltaics

Chun-Che Lee, Wen-Yao Huang

Department of Photonics, National Sun Yat-Sen University, 80424 Kaohsiung City, Taiwan, Republic of China

Received 23 June 2011; accepted 15 September 2011
DOI 10.1002/app.35653
Published online in Wiley Online Library (wileyonlinelibrary.com).

ABSTRACT: Poly(acrylamide) disc-columnar liquid crystals act as a transport interlayer that has been developed to improve photoconversion efficiency. It is composed of 2,3,6,7-tetra-6-hexyloxydibenzo[a,c]phenazine-11-carboxylic monomer and polyacrylamide to show a high isotropic phase transition point of $\sim$ 270°C and a decomposition temperature $T_d^{5\%} = 450$°C. Absorption in the visible light region is in the range of 200–450 nm. A hexagonally columnar mesophase was investigated by optical and texture analysis. The ability of a self-assembled pathway enhanced carrier mobility due to π-π conjugation in stacking up macrocyclic core. This study demonstrated the insertion of a functionally dibenzophenazine-based polymer as a hole-extracting layer with a columnar array in OPVs which is sufficient to promote a 16% increase in the amount of harvested light. © 2012 Wiley Periodicals, Inc. J Appl Polym Sci 000: 000–000, 2012

Key words: hexagonal columnar mesophase; self-arrangement; interlayer; morphology

INTRODUCTION

Bulk heterojunction (BHJ) organic photovoltaics (OPVs) has achieved photoconversion efficiency of around 5% through the blend of an electron-donating conjugated polymer and an electron-accepting fullerene.[1–3] Several factors limit the performance of OPVs. One such factor is the poor alignment of *D/A* (the conjugated polymer poly(3-hexylthiophene)

(P3HT) and the fullerene derivative [6,6]-phenyl-C61-butyric acid methyl ester (PCBM)) molecule orbital levels which results in a small open-circuit voltage (V_{OC}, as a function of band gap that is the maximum voltage available from a solar cell, and this occurs at zero current). Another issue is the unbalanced charge transport, which results in low photocurrent and poor fill factor (FF). Great efforts are being made both in developing new organic materials with low optical band gap and in designing different structural cells for exciton harvesting in the visible light range.[4–9]

Recently, BHJ OPVs with improved performance were achieved by insertion of some conductivity fillers between the active layer (P3HT:PCBM) and the hole-extracting layer (PEDOT:PSS); this resulted in an improved charge injection or collection. Zhang et al.[10,11] demonstrated that the copper phthalocyanine (CuPc) interlayer between blended P3HT/PCBM and PCBM resulted in the improvement of short-circuit current density (J_{SC} in I_{SC}/cm^2; The short-circuit current, I_{SC}, is the current through the solar cell when the voltage across the solar cell is zero), and that power conversion efficiency (PCE) led to balanced carrier injection and reduced hole-leakage to the cathode. Further influence in efficiency is referred to thickness. Lee et al.[12,13] reported that OPV performance could be effectively improved by introducing a thin pentacene interlayer. This provided an additional path for electron transfer that enabled large hole mobility of pentacene and the increased interfacial surface area induced by its pyramid-like morphology. An important aspect of the lowering of the hole injection barriers and interfacial series resistance, or improved optical absorption and photocurrent have been made through attempts to get the buffer layer to ameliorate Ohmic loss (decrease in bulk resistance) in the whole device. For example, an increasing electric field in the photoactive layer with excited localized surface plasmons of Ag nanoparticles was used.[14]

In addition to controlling dimensions on the nanoscale and orientation of the D/A domains there is the challenge to improve photovoltaic performances.[15–18] The use of nanowires in the active layer provides an attractive way to improve transport for the charge carriers. Varied configurations have been investigated for using inorganic semiconducting

Additional Supporting Information may be found in the online version of this article.

Correspondence to: W.-Y. Huang (wyhuang@mail.nsysu.edu.tw).

nanowires such as Ge, ZnO, TiO_2, or fullerene-nanorods. In such devices, the fibrils act as a template for the *D/A* materials implying an organization of the domains; as a consequence, transport properties have been improved.[19–21]

Furthermore, the regularly thin films of self-assembled columnar liquid crystals have been exploited for attaining high performance through the utilization of intermolecular and mesoscopic ordering. An unique one-dimensional charge carrier mobility arise from the columnar axis when self assembled in hexagonal columnar mesophases, whereby the charge mobility of columnar-packed discotic liquid crystals (DLCs) exhibited up to 0.5–1 $cm^2/$ (V s).[22]

In this study, a tetra-hexyloxydibenzo[a,c]phenazine-based monomer attached to the backbone of polyacrylamide (DLC-PAMs) that showed a perpendicular disc-column; furthermore, the suited thickness of a DLC-PAM interlayer between P3HT:PCBM and PEDOT:PSS was provided. This layer acted as a functional interlayer for controlling the organization of the domains to improve light harvest.

EXPERIMENT

Materials

Polyacrylamide (PAMs; $(C_3H_5NO)_n$; ALDRICH) with average molecular weight (M_w) *ca.* 1500 and raw materials were purchased from a commercial source. Commercial reagents and solvents such as Pyridine, *N*,*N*-Dimethylformamide (DMF), Anhydrous dichloromethane, Acetic acid and Dimethyl sulfoxide (DMSO) were distilled and deoxygenated under a nitrogen atmosphere by stirring at 50°C overnight before used. All chemical reactions were performed using standard vacuum-line techniques and dehydrated with a slow stream of nitrogen in the reaction vessel throughout the reaction. These detail process were shown in Supporting Information Scheme 1.

Characterization

Molecular weight characterization was conducted with a Polymer Laboratories gel permeation chromatography (GPC) system using polystyrene as a standard and tetrahydrofuran as the eluent. UV-Vis absorption spectra were recorded using a Perkin Elmer Lambda 35 spectrophotometer. A polarized optical microscope (POM, Nikon ECLIPSE LV100POL) was employed to observe the morphological textures of the DLC thin films, and optical anisotropy properties were identified with a home built set-up shown in Supporting Information, by rotating the sample angle when detecting light penetration. The surface morphologies on the nanometre scale were characterized using a scanning electron microscope (SEM) and atomic force microscopy (AFM). The X-ray diffraction (XRD) measurements were performed using a Philips X'PertPro diffractometer. A radiation source derived from a monochromatic CuKα beam with a wavelength of $\lambda = 0.154$ nm was applied. The detector scanned at small angle (2θ) in a plane defined by the incident beam and the normal surface. The work functions of these materials in air were measured through photoelectron spectroscopy (PESA, AC-2).

Cell fabrication

The devices were fabricated on patterned indium tin oxide (ITO) coated glass substrates with a sheet resistance of 20 $\Omega/\square$. After routine solvent cleaning, the substrates were coated with a 60 nm layer of poly(3,4-ethylenedioxythiophene) (PEDOT): poly (styrenesulfonate) (PSS), followed by baking at 180°C for 10 min. However, the DLC-PAMs were prepared via spin-casting onto a PEDOT: PSS layer to form thin films in various thicknesses. Then, a thermo-treatment was processed at an isotropic temperature of 220°C and then cooled under nitrogen at the rate of 1°C/min to form a columnar stack. For the active layer, a 100-nm thickness of the P3HT: PCBM (1 : 1, w/w) blend was then spin-cast from an *o*-xylene solution and dried for 10 min at 130°C. Finally, a 200-nm thick aluminum top electrode was deposited under vacuum through a shadow mask. The active area of OPVs displayed an oblong shape of 12 mm^2.

The thickness of each layer was controlled by changing the spin speed and solution concentration. The thickness and the spin-casted rate were calibrated with a variation of ± 5 nm by an ellipsometry and a surface profiler (Dektak, Veeco Instruments), respectively, before preparation of the test samples for OPVs. The Al cathode and the deposition rate were monitored by a quartz-crystal microbalance during the thermal evaporation process. For comparison, by controlling film-forming conditions, the standard for OPVs without DLC-PAMs insertion was also fabricated with the same thicknesses and conditions.

Photocurrent–voltage measurements were recorded with a Keithley 2400 source meter. A solar simulator (NewPort, model Oriel 91160) equipped with a 300 W xenon lamp (model 6258) was used as a light source to realize AM1.5G conditions (100 mW/cm^2), where light intensity was adjusted using a National Renewable Energy Laboratory (NREL)-calibrated mono Si solar cell with a KG-3 filter.

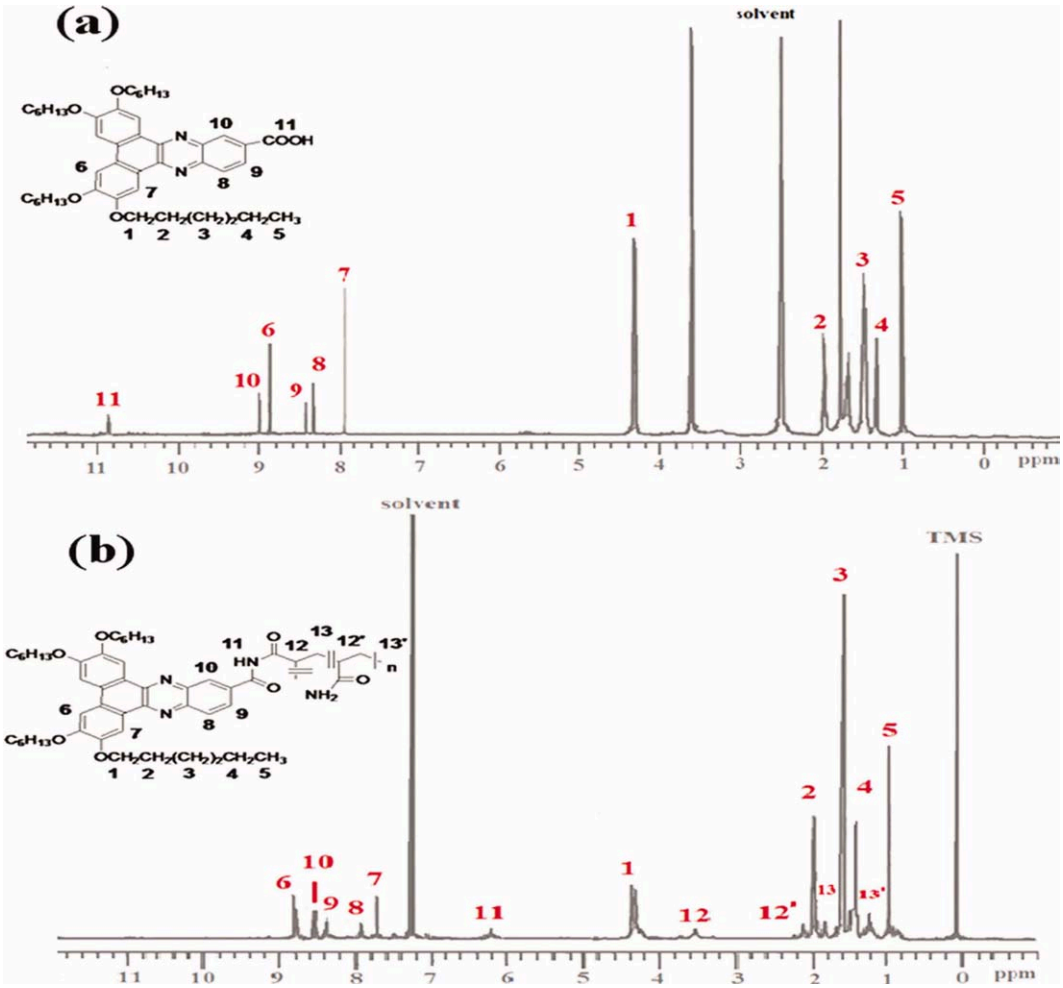

Figure 1 ^{1}H NMR spectra. (a) DLCs, (b) DLC-PAMs. [Color figure can be viewed in the online issue, which is available at wileyonlinelibrary.com.]

RESULTS AND DISCUSSION

The precursors and DLC-PAMs were prepared by a modified procedure as outlined in Supporting Information Scheme 1. The 2,3,6,7-tetra-6-hexyloxydibenzo[a,c]phenazine-11-carboxylic monomer (DLCs) attached onto polyacrylamide (PAMs) with *N,N′*-Dicylohexylcarbodiimide, 4-Dimethylaminopyrdine and anhydrous DMSO in good yield. Gel permeation chromatography was used to determine the molecular weight of DLC-PAMs soluble in tetrahydrofuran (THF); the results showed polystyrene equivalent M_w to be 12,000 and the polydispersity index (PDI), 1.32.

The ^{1}H-NMR spectroscopic data (Fig. 1) identified the molecular structures of both the disc-columnar liquid crystal and the derivate DLC-PAMs. The ^{1}H-NMR spectrum [Fig. 1(a)] of the DLCs showed a signal at 10.9 ppm that attributed to the proton of the carboxylic acid group. The corresponding ^{1}H-NMR spectrum of the polymer DLC-PAMs after the connecting reaction is shown in Figure 1(b) and presents two signals at 3.5 and 2.1 ppm that ascribed to the tertiary protons 12 and 12′ of the attached and nonattached to PAMs, respectively. The signal at 10.9 ppm caused by the carboxylic acid group of the DLCs completely disappeared due to amide formation. In addition, the ratio of the attachment to PAMs could be extracted accordingly via the signal area integration of the tertiary protons 12 and 12′. The result showed the connected percentage to be around 50 mol %, which is consistent with the results of molecular weight measurement. Other qualitative analysis such as Fourier transform infrared spectroscopy (FTIR) and FAB-Mass are revealed in Supporting Information.

Thermal properties were investigated using thermogravimetric analysis and differential scanning calorimetry (Supporting Information Figs. 3 and 4). The thermal transitions of each sample are summarized in Table I. In the DSC scan of DLCs and DLC-PAMs with a heating rate of 15°C/min and nitrogen stream

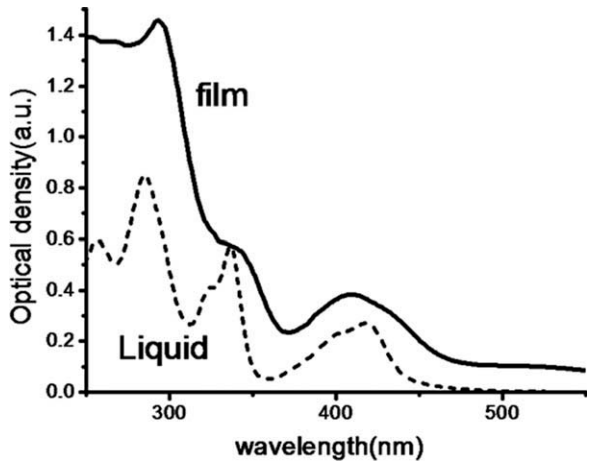

Figure 2 UV absorption spectra of DLC-PAMs.

of 20 cm^3/min, only the DLC endothermic transition clearly showed the point of T_g (160°C), T_i (260°C), and T_m (174°C respectively) indicated as solid-to-liquid crystals, liquid crystal-to-isotropic liquid transitions and melting phase. The thermal scan of DLC-PAMs revealed a broad endothermic event beginning as an increase in the isotropic melt of specific heat follow. At higher temperatures, the mesophase transition of DLC-PAMs was ascribed to side chain motion, representing a mesophase transition whereby the polymer chain hindered the translational motion of the rod. The endotherm of transformation of the mesophase was caused by the orientation and coincided with the isotropization temperature observed in POM. In Supporting Information Figure 3, the TGA thermograms show the decomposition processes for DLC-PAMs. The first process, starting at about 415°C with a weight loss of 4%, was attributed to the degradation of nonconnected PAMs. The second process, starting at about 420°C with char residue of 32% at 900°C, was ascribed to the degradation of the DLC-attached PAMs. The initial thermal degradation temperature of about 420°C was well above the highest temperature (350°C) used in the DSC experiments.

Figure 2 reveals the absorption properties of the DLC-PAMs in a liquid state and as a solid film, thus indicating its ability to absorb light in the visible region. The absorption of DLC-PAMs in DMSO (2×10^{-4} *M*) exhibited three peaks (λ_{max}) of 280, 330, and 425 nm due to π-π* transitions in the conjugated core. The solid film revealed the λ_{max} at the range of 310, 340, and 420 nm with a broaden distribution. The influence of the polymer-chain illustrated a significant difference in absorption within a distinct stoke shift and broadening phenomenon at the ultraviolet region while aggregating from liquid state to solid film. Interestingly, the solid film underwent similar n-đ* and π-π* transitions. There were intramolecular and supramolecular interactions on the

TABLE I
Phase Transition and Decomposition Temperature[a]

	[b]T_g	[b]T_i	[b]T_m	[c]$T_d^{5\%}$
DLCs	170	260	174	423
DLC-PAMs	nd	275	nd	443

[a] The system of units: °C.
[b] Investigation of 2nd heating and cooling flow with DSC.
[c] Thermal degradation temperature at 5% weight loss collected from TGA.

cylindrical stack due to a polymer-chain that imposed a larger geometric effect on the groundstate electronic structure of DLCs, while it was naturally aggregated and self-arranged.

The determination of supramolecular structures for DLCs and poly(acrylamide) disc columnar LCs were investigated by X-ray diffraction with thin films. Figure 3 shows a supramolecular structures of DLC-PAMs were collected by X-ray diffraction with spin-casted films, using three samples of glass/ITO, glass/ITO/PEDOT:PSS and glass/ITO/PEDOT:PSS/DLCPAM, respectively. For Figure 3(a), The corresponding *d* spacings were calculated with the reciprocal spacing following a ratio of $1/\sqrt{3}$, and 3.41 Å of the intermolecular π-stack distance (the distances of two tabulated macrocyclic planes). These results implied a typically hexagonal columnar mesophase that agreed with a previous report.[23,24] For comparison, Figure 3(b,c) indicated the difference without the inserted DLC-PAM layer. The DLC-PAMs

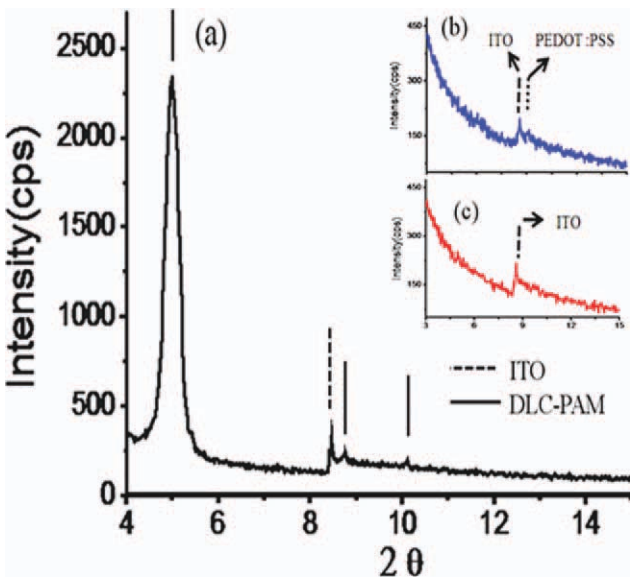

Figure 3 The supramolecular structures of DLC-PAMs were investigated by X-ray diffraction with spin-casted films. (a) glass/ITO/ PEDOT:PSS/ DLCPAMs, (b) glass/ITO/ PEDOT:PSS and, (c) glass/ ITO. [Color figure can be viewed in the online issue, which is available at wileyonlinelibrary.com.]

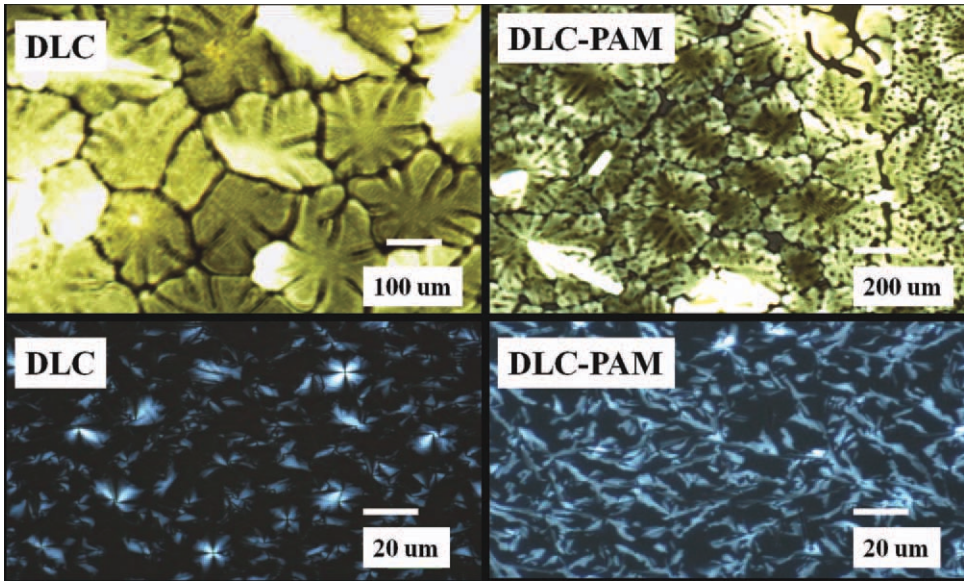

Figure 4 Mesomorphous phases of hexagonal and columnar liquid crystal collected by Polarizing Optical Microscope. [Color figure can be viewed in the online issue, which is available at wileyonlinelibrary.com.]

indicated by X-ray diffraction strongly suggested the presence of hexagonal LC structures.[25,26] However, such broad reflections in the wide-angle region suggested the presence of liquid crystalline orientation with a specific mesophase. This further encouraged our examination of these compounds by Polarized Optical Microscopy, which revealed the mesophases for solid films.

Figure 4 provides the optical textures of the hexagonal columnar liquid-crystal phase determined

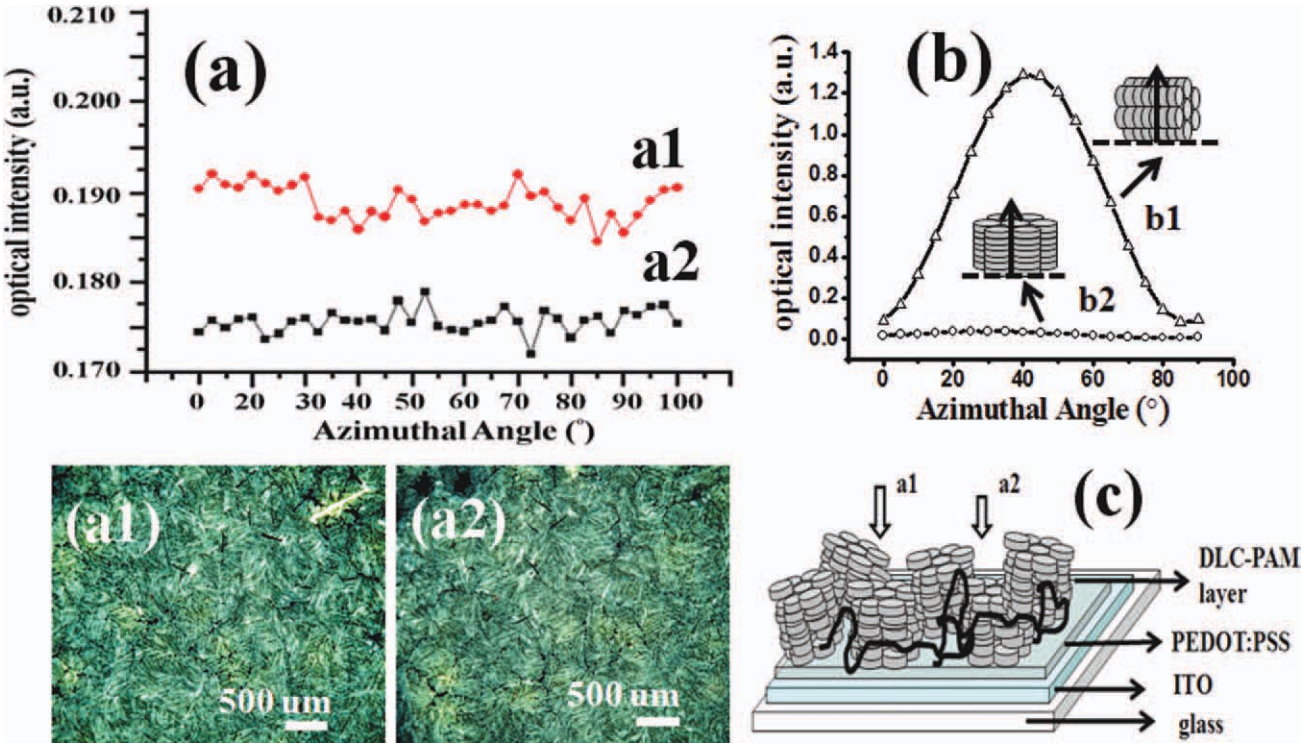

Figure 5 Investigations of self-arranged DLC-PAMs in orientational or positional order. (a) Texture of DLC-PAMs by Polarizing Optical Microscope. Tested position a1 and a2 show in assumptive drawing. (b) Analyses of face-on and edge-on stack capture from optical anisotropy measurement. (c) Assumption of face-on orientation for glass/ ITO/ PEDOT:PSS/ DLC-PAMs. [Color figure can be viewed in the online issue, which is available at wileyonlinelibrary.com.]

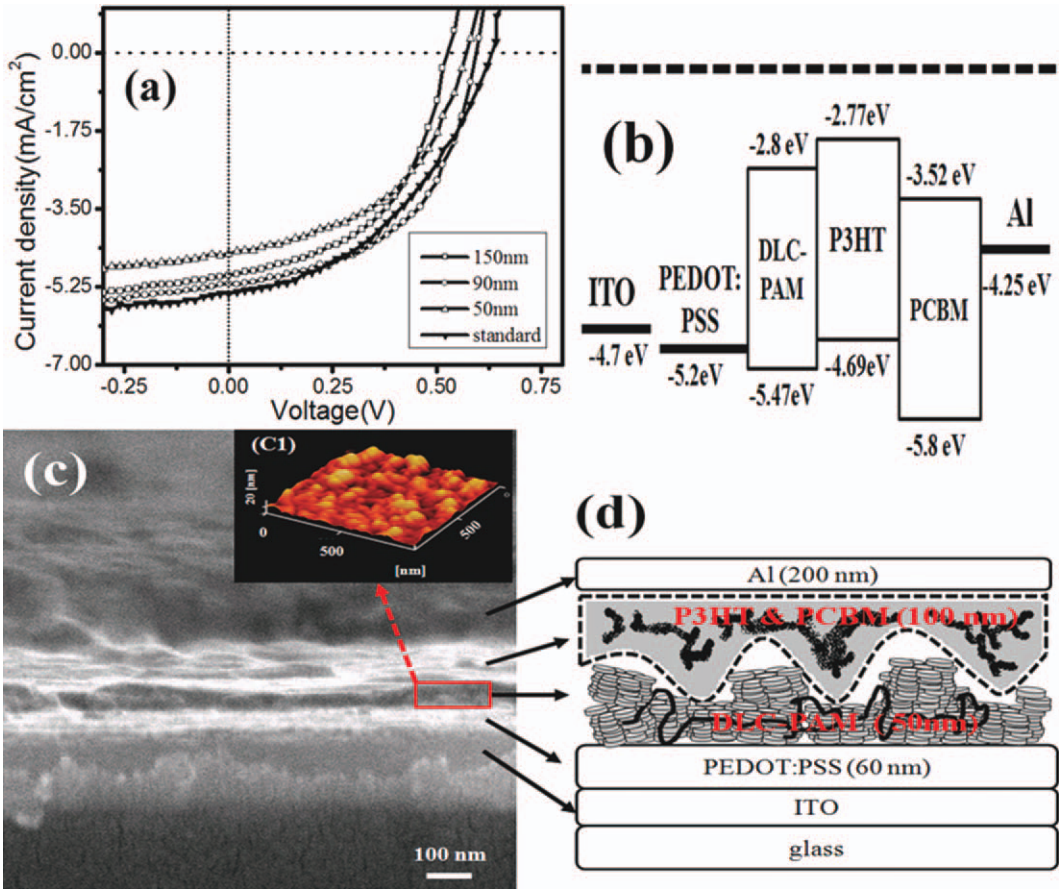

Figure 6 Application of organic thin film solar cell. (a) Performance of light harvest in different thickness of inserted DLC-PAMs. (b) Individual energy diagram for glass/ITO/PEDOT:PSS/DLC-PAMs/P3HT:PCBM/Al. (c) Cross sectional SEM pattern of glass/ ITO/ PEDOT:PSS/ DLC-PAMs and, (c1). AFM pattern in perpendicular columnar array. (d) Cross sectional illustration of OPV device. [Color figure can be viewed in the online issue, which is available at wileyonlinelibrary.com.]

using a Polarizing Optical Microscope. This was investigated at 30°C while cooling down from the isotropic temperature. There were typically fan-shaped textures in both DLCs and DLC-PAMs. A better explanation of the mesophase is based on the rigid DLC monomer possessing a hydrogen carboxyl group, amine/amino, and carbonyl group. Evidently, the enhancement of intermolecular π-stack attractions resulted from the dibenzophenazine macrocyclic core, columnar shape and space-filling effects. This aspect was well in agreement with core size and chain effect.[23–26] For side-chains polymer intertwining, the DLC-PAMs tend to provide an imperfect shape with pin holes and a high transition temperature. Compared with the DLC monomer, there was a blurred Malta cross in DLC-PAM images.[27,28] Further POM information shows in Supporting Information (Figs 5–7) that describe the photomicrographs of dynamic phase transition for DLCs and DLC-PAMs, respectively. One can observe a typical hexagonally columnar mesophase and various phase transitions at different temperatures. Additionally, the morphology of DLC-PAMs which was spin-casted on PEDOT:PSS shows exquisite branches which imply an enhancement of the carrier mobility due to decreased diffusion length in dark field.

To investigate self-arrangement, Figure 5 shows the results of a 90-nm film preparing by controlled spin-casting rate that was annealed to an isotropic temperature of 220°C, subsequently cooled and holed for 30 min at 30°C to achieve orientational or positional order. The sample was subsequently confirmed by optical anisotropy measured through penetrated visible light as indicated in the set-up shown (Supporting Information Fig. 8). In Figure 5(a), showing an inspection of position a1 and a2, the DLC-PAMs showed a rugged line that implies a face-on arrangement with a slight dip due to side-chain entwining. Depending on the angle rotation, a simulated face-on orientation should yield a smooth line segment. There were shown analyses and assumptions in Figure 5(b,c). Observations of POM textures further indicated regular clusters, proving the disc-shaped orientation of DLC-PAMs on a plate. Evidently, it revealed a

TABLE II
Photovoltaic Performance of Organic Thin Film Solar Cell

	DLC-PAM thickness (nm)	V_{oc} (V)	J_{sc} (mA/cm^2)	FF	V_{max} (V)	J_{max} (mA/cm^2)	[c]η (%)
[a]Std	–	0.62	5.36	0.41	0.38	3.62	1.38
[b]DLC-PAM	150	0.52	4.99	0.51	0.38	3.46	1.32
insertion	90	0.60	5.18	0.51	0.42	3.80	1.60
	50	0.58	4.51	0.47	0.40	3.07	1.23

[a] Std: glass/ITO/PEDOT:PSS/P3HT:PCBM/Al.
[b] Device configuration: glass/ITO/PEDOT:PSS/DLC-PAM/P3HT:PCBM/Al.
[c] $\eta\ \% = P_{out}/P_{in}\ \% = (FF \times V_{oc} \times I_{sc})/\text{Pin}\ \% = (V_{max} \times J_{max})/\text{Pin}\%$

regularly perpendicular disc-column of DLC-PAMs which acts as a template to enhance carrier mobility and decrease photocurrent leakage in OPVs.

Figures 6(a,b) illustrate the light harvest of OPVs with different DLC-PAM thicknesses and the energy diagram of the proposed tandem OPVs with the highest occupied molecular orbital (HOMO) and lowest unoccupied molecular orbital (LUMO) parameters. A real device was observed by the cross-sectional view of SEM and AFM images in Figure 6(c). The configuration of OPVs, shown in Figure 6(d), indicates the DLC-PAMs acting as an interlayer or a template in the device. The geometrical structure enabled the functions of DLC-PAM layer to enhance carrier mobility with perpendicular columnar stacks. As a template, a good control of morphology between the active layer and the DLC-PAMs implied that the interface could affect the diffusion length to improve the fill factor in OPVs. Essentially, excitons and holes were collected and dissociated at the interfaces in the "Finger structure" of DLC-PAM template, suggesting a carrier extracting and transporting media. This structure can be regarded as a parallel connection of two individual subcells which reduces bulk resistance due to the circuit model.

In Table 2, we described parameters of OPVs under Air Mass 1.5 Global illumination and irradiation of 100 mW/cm^2. For the optimized thicknesses, the maximum photovoltage (V_{max}), fill factor (FF), and maximum photocurrent (J_{max}) of 90-nm DLC-PAM interlayer presented a higher degree than STD devices, leading to about 20% increase in magnification efficiency (η). This is consistent with the simulation results from the optima exciton diffusion length of about 100 nm. According to the working principles of multilayer OPVs, with an unsuited DLC-PAM layer (flimsy thickness), some excitons will be lost and not contribute to the photocurrent. A very thick DLC-PAM layer will increase the series resistance and hinder carrier transport. Effectively, due to overlapping in the absorption spectra, the DLC-PAMs will increase the amount of excitons, thus enhancing the light harvest of OPVs.

The changes in geometrical configuration, series resistance and fill factor imply that additional interfaces in the OPVs influence the charge transport that increase the photoconversion efficiency (η) up to 1.6%. It is expected that further study of carrier transport in this structure will continuously improve device performance.

In summary, the experimental results demonstrated the influences of an interlayer as a template in organic photovoltaics. The layer of poly(acrylamide) disc-columnar liquid crystals led to an increase in the amount of light harvested. In the following summary, a qualitative discussion on the characteristics of DLC-PAMs as it applies to OPVs was described based on the parameters of self-arrangement, morphology of interface, hole extracting, and transporting ability.

1. Self-arrangement: the self-arranged stability of DLC-PAMs refers to the rigid core. The columnar/hexagonal mesophases promoted good orientation and perpendicular columnar array. Hence, the enhancement of OPV performance is ascribed to intense arrangement.
2. Finger structure: Significantly, DLC-PAMs act as a functional template that led to control of the morphology of the interface between the active layer and PEDOT:PSS for reducing diffusion length. Herein, polymer LCs inserted into OPVs, a natural phase separation and short diffusion length led to improved performance.

To provide a detailed understanding of the effect of poly(acrylamide) disc-columnar liquid crystal characteristics as a buffer layer in OPVs, a theoretical analysis is required and is in progress.

CONCLUSION

We demonstrated a possible interlayer with poly (acrylamide) disc-columnar liquid crystals in hexagonal mesophases as a transmittal template for inserting into OPV devices. A self-arranged ability was in an orientational or positional order such as

perpendicular columnar array that brought higher photoconversion efficiency due to improved bulk resistance, carrier mobility and photocurrent leakage. Additionally, an effectively suited thickness for the DLC-PAM interlayer also has been provided.

References

1. Li, G.; Shrotriya, V.; Huang, J.; Yao, Y.; Moriarty, T.; Emery, K.; Yang, Y. Nat Mater 2005, 4, 864.
2. Ma, W. L.; Yang, C. Y.; Gong, X.; Lee, K.; Heeger, A. J. Adv Funct Mater 2005, 15, 1617.
3. Kim, J. Y.; Lee, K.; Coates, N. E.; Moses, D.; Nguyen, T. Q.; Dante, M.; Heeger, A. J. Science 2007, 317, 222.
4. Schilinsky, P.; Waldauf, C.; Bradec, C. J. Appl Phys Lett 2002, 81, 3885.
5. Gebeyehu, D.; Pfeiffer, M.; Maennig, B.; Drechsel, J.; Werner, A.; Leo, K. Thin Solid Films 2004, 451–452, 29.
6. Sullivan, P.; Heutz, S.; Schultes, S. M.; Jones, T. S. Appl Phys Lett 2004, 84, 1210.
7. Hori, T.; Moritou, H.; Fukuoka, N.; Sakamoto, J.; Fujii, A.; Ozaki, M. Materials 2010, 3, 4915.
8. Han, Y.-K.; Chang, M.-Y.; Huang, W.-Y.; Pan, H.-Y.; Ho, K.-S.; Hsieh, T.-H.; Pan, S.-Y. J Electrochem Soc 2011, 158, K88.
9. Bejbouji, H.; Vignau, L.; Miane,J.; Dang, M.-T.; Oualim, E.; Harmouchi, M.; Mouhsen, A. Solar Energy Mater Solar Cells 2010, 94, 176.
10. Zhang, C.; Tong, S. W.; Jiang, C.; Kang, E. T.; Chan, D. S. H.; Zhu, C. Appl Phys Lett 2008, 92, 083310.
11. Zhang, C.; Tong, S. W.; Jiang, C.; Kang, E. T.; Chan, D. S. H.; Zhu, C. Appl Phys Lett 2008, 93, 043307.
12. Kim, J. H.; Huh, S. Y.; Kim, T. I.; Lee, H. H. Appl Phys Lett 2008, 93, 143305.
13. Zhang, F.; Li, Y.; Tang, W.; Wang, J.; Xu, X.; Zhuo, Z.; Xu, Z.; Wang, Y.; Carroll, D. Thin Solid Films 2011, 520, 676.
14. Yoon, W.-J.; Jung, K.-Y.; Liu, J.; Duraisamy, T.; Revur, R.; Teixeira, F. L.; Sengupta, S.; Berger, P. R. Solar Energy Mater Solar Cells 2010, 94, 128.
15. Huang, W. Y.; Lee, C. C.; Hsieh, T. L. Solar Energy Mater Solar Cells 2009, 93, 382.
16. Huang, W. Y; Lee, C. C.; Wang, S. G.; Han, Y. K.; Changa, M. Y. J Electrochem Soc 2010, 157, B1336.
17. Ma, W.; Gopinathan, A.; Heeger, A. J. Adv Mater 2007, 19, 3656.
18. Ma, W.; Yang, C.; Heeger, A. J. Adv Mater 2007, 19, 1387.
19. Ko, D.-H.; Tumbleston, J. R.; Schenck, W.; Lopez, R.; Samulski, E. T. J Phys Chem C 2011, 115, 4247.
20. Wang, M.; Li, Y.; Huang, H.; Peterson, E. D.; Nie, W.; Zhou, W.; Zeng, W.; Huang, W.; Fang, G.; Sun, N.; Zhao, X.; Carroll1, D. L. Appl Phys Lett 2011, 98, 103305.
21. Kang, M.-G.; Xu, T.; Park, H. J.; Luo, X.; Guo, L. J. Adv Mater 2010, 22, 4378.
22. Seonju, J.; Younghwan, K.; Byeong-Dae, C.; Harald, A.; Han, Y. S. Appl Phys Lett 2010, 96, 183305.
23. Foster, E. J.; Babuin, J.; Nguyen, N.; Williams, V. E. Chem Commun 2004, 2052.
24. Kaafarani, B. R. Chem Mater 2011, 23, 378.
25. Li, M. H.; Brûlet, A.; Keller, P.; Cotton, J. P. J Mol Struct 1996, 383, 11.
26. Boden, N.; Bushby, R. J.; Donovan, K.; Liu, Q.; Lu, Z.; Kreouzis, T.; Wood, A. Liquid Crystals 2001, 28, 1739.
27. Morales, P.; Lagerwall, J.; Vacca, P.; Laschat, S.; Scalia, G. J Org Chem 2010, 6, 51.
28. Kumar, S. Chemistry of Discotic Liquid Crystals: From Monomers to Polymers. ISBN-13: 9781439811436.